



# Highly efficient dual anthracene core derivatives through optimizing side groups for blue emission



Hayoon Lee<sup>a,1</sup>, Minjin Jo<sup>b,1</sup>, Garam Yang<sup>b</sup>, Hyocheol Jung<sup>a</sup>, Seokwoo Kang<sup>a</sup>, Jongwook Park<sup>a,\*</sup>

<sup>a</sup> Department of Chemical Engineering, College of Engineering, Kyung Hee University, Youngin, Gyeonggi, 17104, Republic of Korea

<sup>b</sup> Department of Chemistry, The Catholic University of Korea, Bucheon, Gyeonggi, 14662, Republic of Korea

## ARTICLE INFO

### Article history:

Received 27 April 2017

Received in revised form

23 May 2017

Accepted 21 June 2017

Available online 23 June 2017

### Keywords:

OLED

EML

Blue emission

Core-side concept

9,9'-bianthracene

## ABSTRACT

TP-AA-TPB, TP-AA-TPB, TPB-AA-TPB, TP-AA-DPA, TP-AA-TPA, and TPB-AA-TPA were synthesized using a 9,9'-bianthracene (AA core). Through a systematic side group change, we optimized the dual-core chromophore system and investigated the relationship between the core and the side groups. The ultraviolet-visible (UV-Vis) absorption of the six materials showed an intrinsic absorption peaks of anthracene in the range of 360 nm–410 nm and photoluminescence (PL) emission in the blue region. The minimum decomposition temperatures ( $T_d$ ) was 425 °C, the minimum melting temperatures ( $T_m$ ) was 335 °C, and the minimum glass transition temperatures ( $T_g$ ) was 176 °C. We achieved excellent overall electroluminescence (EL) efficiency in non-doped OLED devices using the six synthesized materials as emitting layer (EML). TPB-AA-TPA synthesized through size and polarity optimization of the side groups on the AA core had a current efficiency of 8.97 cd/A, power efficiency of 4.43 lm/W, external quantum efficiency (EQE) of 6.37%, and Commission Internationale de L'Eclairage coordinates (CIE) of (0.14, 0.19). TPB-AA-TPA also maintained blue emission and realized the highest EL efficiency among the six synthesized materials.

© 2017 Published by Elsevier Ltd.

## 1. Introduction

Since the first reported organic light-emitting diodes (OLEDs) by Tang and Van Slyke, OLEDs are now attracting attention in the market, such as for mobile phone and TV display and solid-state lighting because of their potentials as next generation applications [1]. These OLEDs require red, green, and blue emitting materials to realize a full color display. In particular, blue emitting materials require a wide energy band gap, which causes high charge injection barriers in the device, thus blue OLED devices are relatively inferior to green and red in terms of electroluminescence (EL) efficiency and device lifetime [2–15].

The emitting materials can be divided into fluorescent materials and phosphorescent materials. In the case of a blue-emitting material with a wide energy band gap, fluorescent materials show higher efficiency, greater color gamut, and a longer lifetime than phosphorescent materials [16]. The phosphorescent blue-emitting

material should use a lower triplet energy level ( $T_1$ ) than the singlet energy level ( $S_1$ ) of the fluorescent material, and it is difficult to develop a phosphorescent blue emitting material because of the limits in achieving a molecular structure with a high  $T_1$  level [17,18].

In order to solve these problems, many fluorescent blue-emitting materials have been synthesized to improve the efficiency and the long lifetime. However, development of blue emitting materials with a pure color and high efficiency is still required. We systematically designed the structure of a fluorescent emitting material, synthesized it using the core-side concept, and reported the properties accordingly [9,10,19]. The core group is responsible for the main absorption and emission roles of the final compound, and the side groups capable of controlling the size, arrangement, and polarity of the final molecule are symmetrically or asymmetrically arranged.

We have also reported a systematic study of the derivatives of dual and triple cores composed of two or three chromophores compared to single core group derivatives [11,12,20,21]. In the case of a dual core, relatively higher quantum efficiency is shown in photoluminescence (PL) and EL compared to a single core, and the

\* Corresponding author.

E-mail address: [jongpark@khu.ac.kr](mailto:jongpark@khu.ac.kr) (J. Park).

<sup>1</sup> Hayoon Lee and Minjin Jo contributed equally to this work as the first coauthor.

results of the research on relatively longer lifetime and its theoretical explanation are also reported. Dual core and triple core studies have been reported using anthracene and pyrene groups. However, this study proposes a homogeneous dual core system. A homogeneous dual core can be composed of chromophore such as anthracene, pyrene, chrysene, carbazole, or fluorene. Among these, anthracene is a representative blue chromophore with a wide band gap, high fluorescence quantum yield, and good thermal stability.

In this study, we used anthracene group as a homogeneous dual core. The homogeneous dual core used here is 9,9'-bianthracene, defined as the AA core, and differs from conventional heterogeneous dual core chromophores. In the AA core, two anthracenes are connected to a single bond at the 9 and 9' positions. According to the crystallographic information, the dihedral angle formed by the two anthracene is approximately 89.4° due to strongly repulsive hydrogen atoms located at the 1,1' and 8,8' positions [22]. In addition, in an electronically decoupled structure with an orthogonal structure in the ground state, like the AA core, strong electronic interaction is observed for the relaxed state of the excited state [23–25]. Thus, the AA core can have its own high PL efficiency.

Aromatic side groups with different sizes and aromatic amine side groups with the electron donating effect were used on the AA core, unlike in previous studies. We also studied side group optimization for the AA core by systematically changing the side group symmetrically or asymmetrically. The *m*-terphenyl group (TP) and triphenylbenzene (TPB) were used as bulky aromatic side groups, and diphenylamine (DPA) and triphenylamine (TPA) were used as aromatic amine side groups with the electron donating effect. The six materials synthesized were 10,10'-di([1,1':3',1''-terphenyl]-5'-yl)-9,9'-bianthracene (TP-AA-TP); 10-([1,1':3',1''-terphenyl]-5'-yl)-10'-(5'-phenyl-[1,1':3',1''-terphenyl]-4-yl)-9,9'-bianthracene (TP-AA-TPB); 10,10'-bis(5'-phenyl-[1,1':3',1''-terphenyl]-4-yl)-9,9'-bianthracene (TPB-AA-TPB); 10'-([1,1':3',1''-terphenyl]-5'-yl)-N,N-diphenyl-[9,9'-bianthracen]-10-amine (TP-AA-DPA); 4-(10'-([1,1':3',1''-terphenyl]-5'-yl)-[9,9'-bianthracen]-10-yl)-N,N-diphenylaniline (TP-AA-TPA); N,N-diphenyl-4-(10'-(5'-phenyl-[1,1':3',1''-terphenyl]-4-yl)-[9,9'-bianthracen]-10-yl)aniline (TPB-AA-TPA) (Scheme 1).

## 2. Experimental

### 2.1. Synthesis

<sup>13</sup>C NMR data of the Type (B) materials could not be obtained because of the very low solubilities.

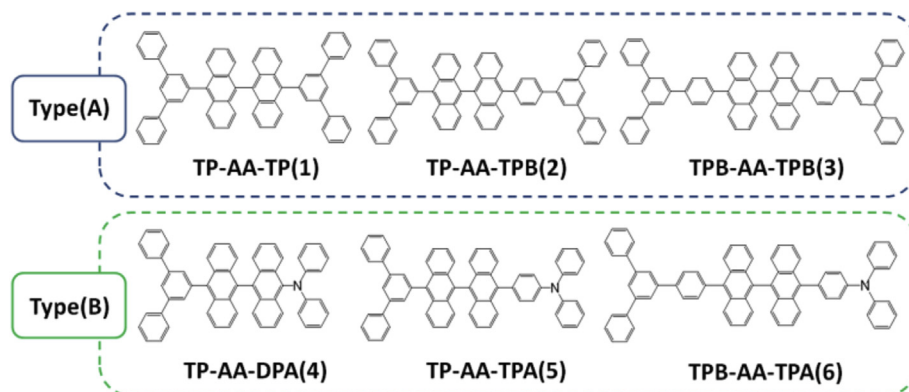
**Compound [1] 5'-bromo-1,1':3',1''-terphenyl** 1,3,5-tribromobenzene (10 g, 30.60 mmol), phenylboronic acid (8.22 g,

67.32 mmol), and Pd(PPh<sub>3</sub>)<sub>4</sub> (2.12 g, 1.84 mmol) were added to anhydrous tetrahydrofuran (THF) solution (200 mL) under nitrogen. Then, 2 M K<sub>2</sub>CO<sub>3</sub> solution (95 mL) dissolved in H<sub>2</sub>O was added to the reaction mixture at 50 °C. The mixture was refluxed for 4 h. After the reaction was complete, the reaction mixture was extracted with chloroform and water. The organic layer was dried with anhydrous MgSO<sub>4</sub> and filtered. The solution was evaporated. The product was isolated with silica gel column chromatography using chloroform: n-hexane (1:20) as the eluent to obtain a white solid (5.68 g, 60%). <sup>1</sup>H NMR (300 MHz, CDCl<sub>3</sub>, 25 °C, TMS): δ (ppm) 7.70 (s, 3H), 7.62 (d, *J* = 6.9, 4H), 7.47 (t, *J* = 6.9, 4H), 7.39 (t, *J* = 7.2, 2H).

**Compound [2] 2-([1,1':3',1''-terphenyl]-5'-yl)-4,4,5,5-tetramethyl-1,3,2-dioxaborolane** compound [1] (5 g, 16.2 mmol) was added to anhydrous THF solution (200 mL) under nitrogen. Then, 2.0 M *n*-butyllithium (9.7 mL, 19.5 mmol) was added slowly at −78 °C. Next, isopropoxy-4,4,5,5-tetramethyl-1,3,2-dioxaborolane (4.65 mL, 24.3 mmol) was added to the reaction mixture, and the mixture was stirred at room temperature. After the reaction was complete, the reaction mixture was extracted with chloroform and water. The organic layer was dried with anhydrous MgSO<sub>4</sub> and filtered. The mixture was evaporated. The residue was re-dissolved in chloroform and added to excess methanol. The precipitate was filtered and washed with methanol to obtain a white solid (5.19 g, 90%). <sup>1</sup>H NMR (300 MHz, CDCl<sub>3</sub>, 25 °C, TMS): δ (ppm) 8.03 (s, 2H), 7.90 (s, 1H), 7.69 (d, *J* = 6.9, 4H), 7.45 (t, *J* = 7.2, 4H), 7.35 (t, *J* = 7.5, 2H), 1.37 (s, 12H).

**Compound [3] 4-bromo-5'-phenyl-1,1':3',1''-terphenyl** compound [2] (3.5 g, 9.82 mmol), 1,4-dibromobenzene (3.3 g, 13.2 mmol), and Pd(PPh<sub>3</sub>)<sub>4</sub> (0.4 g, 0.34 mmol) were added to anhydrous THF solution (30 mL) under nitrogen. Then, 2 M K<sub>2</sub>CO<sub>3</sub> solution (3.0 mL) dissolved in H<sub>2</sub>O was added to the reaction mixture at 50 °C. The mixture was refluxed overnight under nitrogen. After the reaction was complete, the reaction mixture was extracted with chloroform and water. The organic layer was dried with anhydrous MgSO<sub>4</sub> and filtered. The solution was evaporated. The product was isolated with silica gel column chromatography using chloroform: n-hexane (1:5) as the eluent to obtain a white solid (2.01 g, 53%). <sup>1</sup>H NMR (300 MHz, [D<sub>6</sub>]DMSO, 25 °C, TMS): δ (ppm) 7.90–7.84 (m, 9H), 7.70 (d, *J* = 8.7, 2H), 7.51 (t, *J* = 7.2, 4H), 7.41 (t, *J* = 7.2, 2H).

**Compound [4] 9,9'-bianthracene** anthraquinone (10 g, 48 mmol) and zinc powder (25 g, 33 mmol) were dissolved in acetic acid (240 mL). Then, HCl (60 mL) was added slowly at 50 °C. The mixture was refluxed overnight. After the reaction was complete, the mixture was cooled at room temperature. The mixture was filtered and washed with methanol. The residue was re-dissolved in chloroform and added to excess ethanol. The precipitate was



Scheme 1. Chemical structures of the synthesized compounds.

filtered and washed with ethanol to obtain a beige solid (5.10 g, 30%). <sup>1</sup>H NMR (300 MHz, CDCl<sub>3</sub>, 25 °C, TMS): δ (ppm) 8.68 (s, 2H), 8.16 (d, *J* = 8.7, 4H), 7.44 (t, *J* = 7.8, 4H), 7.16–7.06 (m, 8H).

**Compound [5] 10,10'-dibromo-9,9'-bianthracene** compound [4] (5.0 g, 14.1 mmol) and N-bromosuccinimide (NBS), (5.52 g, 31.0 mmol) were added to chloroform (300 mL), and then acetic acid (50 mL) was added to the reaction mixture. The mixture was refluxed for 3 h. After the reaction was complete, the reaction mixture was extracted with chloroform and water. The organic layer was dried with anhydrous MgSO<sub>4</sub> and filtered. The solution was evaporated. The residue was re-dissolved in chloroform and added to excess ethanol. The precipitate was filtered and washed with ethanol to obtain a yellow solid (6.64 g, 92%). <sup>1</sup>H NMR (300 MHz, CDCl<sub>3</sub>, 25 °C, TMS): δ (ppm) 8.72 (d, *J* = 9.0, 4H), 7.58 (t, *J* = 7.5, 4H), 7.18 (t, *J* = 9.0, 4H), 7.08 (d, *J* = 7.5, 4H).

**Compound [6] 10,10'-bis(4,4,5,5-tetramethyl-1,3,2-dioxaborolan-2-yl)-9,9'-bianthracene** compound [5] (10 g, 19.5 mmol) was added to anhydrous THF solution (400 mL) under nitrogen. Then, 2.0 M n-butyllithium (22 mL, 39.2 mmol) was added slowly at –78 °C. Next, isopropoxy-4,4,5,5-tetramethyl-1,3,2-dioxaborolane (8.0 mL, 39.2 mmol) was added to the reaction mixture and stirred at room temperature. After the reaction was finished, the reaction mixture was extracted with chloroform and water. The organic layer was dried with anhydrous MgSO<sub>4</sub> and filtered. The mixture was evaporated. The product was isolated with silica gel column chromatography using chloroform: n-hexane (1:2) as the eluent to obtain a white solid (4.26 g, 36%). <sup>1</sup>H NMR (300 MHz, CDCl<sub>3</sub>, 25 °C, TMS): δ (ppm) 8.50 (d, *J* = 8.7, 4H), 7.43 (t, *J* = 7.8, 4H), 7.10–7.02 (m, 8H), 1.65 (s, 24H).

**Compound [7] 10-bromo-9,9'-bianthracene** compound [4] (5.0 g, 14.1 mmol) and NBS (2.76 g, 15.5 mmol) were added to chloroform (300 mL), and acetic acid (15 mL) was added to the reaction mixture. The mixture was refluxed for 2 h. After the reaction was complete, the reaction mixture was extracted with chloroform and water. The organic layer was dried with anhydrous MgSO<sub>4</sub> and filtered. The solution was evaporated. The residue was re-dissolved in chloroform and added to excess ethanol. The precipitate was filtered and washed with ethanol to obtain a yellow solid (4.89 g, 80%). <sup>1</sup>H NMR (300 MHz, [D<sub>8</sub>]THF, 25 °C, TMS): δ (ppm) 8.78 (s, 1H), 8.70 (d, *J* = 9.0, 2H), 8.19 (d, *J* = 8.4, 2H), 7.59 (t, *J* = 7.8, 2H), 7.46 (t, *J* = 7.8, 2H), 7.21–6.99 (m, 8H).

**Compound [8] 2-([9,9'-bianthracen]-10-yl)-4,4,5,5-tetramethyl-1,3,2-dioxaborolane** compound [7] (10 g, 19.5 mmol) was added to anhydrous THF solution (400 mL) under nitrogen. Then, 11.7 mL of 2.0 M n-butyllithium (23 mmol) was added slowly at –78 °C. Next, 4 mL of isopropoxy-4,4,5,5-tetramethyl-1,3,2-dioxaborolane (27.3 mmol) was added to the reaction mixture and stirred at room temperature. After the reaction was complete, the reaction mixture was extracted with chloroform and water. The organic layer was dried with anhydrous MgSO<sub>4</sub> and filtered. The mixture was evaporated. The product was isolated with silica gel column chromatography using chloroform: n-hexane (1:2) as the eluent to obtain a white solid (3.36 g, 36%). <sup>1</sup>H NMR (300 MHz, CDCl<sub>3</sub>, 25 °C, TMS): δ (ppm) 8.66 (s, 1H), 8.52 (d, *J* = 8.7, 2H), 8.15 (d, *J* = 8.7, 2H), 7.47–7.40 (m, 4H), 7.14–7.05 (m, 8H), 1.66 (s, 12H).

**Compound [9] 10-([1,1':3',1''-terphenyl]-5'-yl)-9,9'-bianthracene** compound [8] (1.25 g, 2.60 mmol), compound [1] (1.02 g, 3.31 mmol), and Pd(PPh<sub>3</sub>)<sub>4</sub> (0.18 g, 0.15 mmol) were added to anhydrous THF solution (150 mL) under nitrogen. Then, 2 M K<sub>2</sub>CO<sub>3</sub> solution (15 mL) dissolved in H<sub>2</sub>O was added to the reaction mixture at 50 °C and refluxed overnight. After the reaction was complete, the reaction mixture was extracted with chloroform and water. The organic layer was dried with anhydrous MgSO<sub>4</sub> and filtered. The solution was evaporated. The product was isolated

with silica gel column chromatography using chloroform: n-hexane (1:5) as the eluent to obtain a white solid (1.27 g, 84%). <sup>1</sup>H NMR (300 MHz, CDCl<sub>3</sub>, 25 °C, TMS): δ (ppm) 8.70 (s, 1H), 8.18 (d, *J* = 8.7, 2H), 8.08 (s, 1H), 7.99 (d, *J* = 8.7, 2H), 7.88 (s, 2H), 7.83 (d, *J* = 8.4, 4H), 7.53–7.32 (m, 10H), 7.21–7.13 (m, 8H).

**Compound [10] 10-([1,1':3',1''-terphenyl]-5'-yl)-10'-bromo-9,9'-bianthracene** compound [9] (1.28 g, 2.2 mmol) and NBS (0.47 g, 2.64 mmol) were added to chloroform (170 mL), and acetic acid (25 mL) was added to the reaction mixture. The mixture was refluxed for 4 h. After the reaction was complete, the reaction mixture was extracted with chloroform and water. The organic layer was dried with anhydrous MgSO<sub>4</sub> and filtered. The solution was evaporated. The residue was re-dissolved in chloroform and added to excess ethanol. The precipitate was filtered and washed with ethanol to obtain a yellow solid (1.41 g, 97%). <sup>1</sup>H NMR (300 MHz, [D<sub>8</sub>]THF, 25 °C): δ (ppm) 8.73 (d, *J* = 9.0, 2H), 8.21 (s, 1H), 7.98 (d, *J* = 9.0, 2H), 7.91–7.87 (m, 6H), 7.63 (t, *J* = 7.5, 2H), 7.48 (t, *J* = 7.5, 4H), 7.40–7.32 (m, 4H), 7.27–7.07 (m, 8H).

**Compound [11] 10-(5'-phenyl-[1,1':3',1''-terphenyl]-4-yl)-9,9'-bianthracene** compound [8] (2.50 g, 5.2 mmol), compound [3] (2.41 g, 6.42 mmol), and Pd(PPh<sub>3</sub>)<sub>4</sub> (0.24 g, 0.21 mmol) were added to anhydrous toluene solution (600 mL) and anhydrous ethanol (400 mL) under nitrogen. Then, 2 M K<sub>2</sub>CO<sub>3</sub> solution (100 mL) dissolved in H<sub>2</sub>O was added to the reaction mixture at 50 °C. After the reaction was complete, the reaction mixture was extracted with chloroform and water. The organic layer was dried with anhydrous MgSO<sub>4</sub> and filtered. The solution was evaporated. The product was isolated with silica gel column chromatography using chloroform: n-hexane (1:5) as the eluent to obtain a white solid (2.40 g, 73%). <sup>1</sup>H NMR (300 MHz, [D<sub>6</sub>]DMSO, 25 °C): δ (ppm) 8.92 (s, 1H), 8.32 (d, *J* = 8.7, 2H), 8.26 (d, *J* = 8.1, 2H), 8.15 (s, 2H), 7.99 (d, *J* = 8.7, 5H), 7.85 (d, *J* = 8.7, 2H), 7.78 (d, *J* = 8.1, 2H), 7.58–7.52 (m, 6H), 7.45 (t, *J* = 7.5, 4H), 7.31–7.21 (m, 4H), 7.01 (t, *J* = 9.3, 4H).

**Compound [12] 10-bromo-10'-(5'-phenyl-[1,1':3',1''-terphenyl]-4-yl)-9,9'-bianthracene** compound [11] (1.4 g, 2.13 mmol) and NBS (0.42 g, 2.34 mmol) were added to chloroform (140 mL), and then acetic acid (20 mL) was added to the reaction mixture. After the reaction was complete, the reaction mixture was extracted with chloroform and water. The organic layer was dried with anhydrous MgSO<sub>4</sub> and filtered. The solution was evaporated. The residue was re-dissolved in chloroform and added to excess ethanol. The precipitate was filtered and washed with ethanol to obtain a beige solid (1.54 g, 98%). <sup>1</sup>H NMR (300 MHz, [D<sub>6</sub>]DMSO, 25 °C): δ (ppm) 8.68 (d, *J* = 8.7, 2H), 8.27 (d, *J* = 8.4, 2H), 8.15 (s, 2H), 7.99 (d, *J* = 8.4, 5H), 7.86 (d, *J* = 8.7, 2H), 7.79–7.72 (m, 4H), 7.56 (t, *J* = 7.2, 4H), 7.45 (t, *J* = 7.2, 4H), 7.38 (t, *J* = 8.7, 2H), 7.28 (t, *J* = 7.5, 2H), 7.12 (d, *J* = 9.0, 2H), 7.01 (d, *J* = 9.0, 2H).

**Compound [13] N,N-diphenyl-4-(4,4,5,5-tetramethyl-1,3,2-dioxaborolan-2-yl)aniline** (4-Bromo-phenyl)-diphenyl-amine (8.0 g, 24.7 mmol) was added to anhydrous THF solution (300 mL) under nitrogen. Then, 2.0 M n-butyllithium (18.54 mL, 25.4 mmol) was added slowly at –78 °C. Next, triethylborate (5.89 mL, 25.4 mmol) was added to the reaction mixture, followed by HCl (4.53 mL, 49.4 mmol) at room temperature. After the reaction was complete, the reaction mixture was extracted with ethyl acetate (EA) and water. The organic layer was dried with anhydrous MgSO<sub>4</sub> and filtered. The mixture was evaporated. The residue was re-dissolved in THF and added to hexane. The precipitate was filtered and washed with hexane to obtain a white solid (5.0 g, 70%). <sup>1</sup>H NMR (300 MHz, [D<sub>8</sub>]THF, 25 °C): δ (ppm) 7.67 (d, *J* = 8.4, 2H), 7.21 (t, *J* = 8.4, 4H), 7.06–6.95 (m, 10H).

**Compound [TP-AA-TP] 10,10'-di([1,1':3',1''-terphenyl]-5'-yl)-9,9'-bianthracene** compound [6] (1.0 g, 1.65 mmol), compound [1] (1.12 g, 3.62 mmol), Pd(OAc)<sub>2</sub> (0.022 g, 0.10 mmol), and tricyclohexylphosphine (0.056 g, 0.20 mmol) were added to anhydrous

toluene (200 mL) and anhydrous ethanol (140 mL) solution. Then, (Et)<sub>4</sub>NOH (20 wt%, 35 mL) was added to the reaction mixture at 50 °C. The mixture was refluxed for 4 h under nitrogen. After the reaction was complete, the reaction mixture was extracted with chloroform and water. The organic layer was dried with anhydrous MgSO<sub>4</sub> and filtered. The solution was evaporated. The product was isolated with silica gel column chromatography using chloroform: n-hexane (1:3) as the eluent to obtain a white solid (0.98 g, 73%). <sup>1</sup>H NMR (300 MHz, [D<sub>8</sub>]THF, 25 °C): δ (ppm) 8.21 (s, 2H), 8.01 (d, *J* = 9.0, 4H), 7.95 (s, 4H), 7.91 (d, *J* = 7.2, 8H), 7.49 (t, *J* = 7.2, 8H), 7.37 (t, *J* = 9.3, 8H), 7.25–7.15 (m, 8H); <sup>13</sup>C NMR (75 MHz, [D<sub>8</sub>]THF, 25 °C): δ (ppm) 142.61, 141.22, 140.73, 138.28, 134.01, 131.98, 130.77, 129.46, 129.24, 128.04, 127.70, 127.35, 126.06, 125.91, 125.29; HRMS (FAB-MS, *m/z*): calcd. for C<sub>64</sub>H<sub>42</sub>, 810.3287; found, 810.3286 [M]<sup>+</sup>. Anal. calcd for C<sub>64</sub>H<sub>42</sub>: C 94.78, H 5.22; found: C 90.19, H 5.34%.

**Compound[TP-AA-TPB] 10-([1,1':3',1''-terphenyl]-5'-yl)-10'-(5'-phenyl-[1,1':3',1''-terphenyl]-4-yl)-9,9'-bianthracene** compound [12] (0.6 g, 0.81 mmol), compound [2] (0.35 g, 0.97 mmol), and Pd(PPh<sub>3</sub>)<sub>4</sub> (0.03 g, 0.024 mmol) were added to anhydrous toluene solution (300 mL) and anhydrous ethanol (200 mL) under nitrogen. Then, 2 M K<sub>2</sub>CO<sub>3</sub> solution (50 mL) dissolved in H<sub>2</sub>O was added to the reaction mixture at 50 °C. After the reaction was complete, the reaction mixture was extracted with chloroform and water. The organic layer was dried with anhydrous MgSO<sub>4</sub> and filtered. The solution was evaporated. The product was isolated with silica gel column chromatography using chloroform: n-hexane (1:3) as the eluent to obtain a white solid (0.55 g, 76%). <sup>1</sup>H NMR (300 MHz, [D<sub>8</sub>]THF, 25 °C): δ (ppm) 8.22 (s, 1H), 8.18 (d, *J* = 8.1, 2H), 8.13 (s, 2H), 8.01–7.87 (m, 15H), 7.78 (d, *J* = 8.1, 2H), 7.53–7.46 (m, 8H), 7.42–7.34 (m, 8H), 7.24–7.15 (m, 8H); <sup>13</sup>C NMR (75 MHz, [D<sub>8</sub>]THF, 25 °C): δ (ppm) 140.61, 140.22, 140.09, 139.27, 138.83, 138.72, 138.34, 136.51, 135.88, 135.73, 131.61, 131.58, 130.01, 129.59, 128.37, 127.08, 126.85, 126.82, 125.65, 125.53, 124.98, 123.68, 123.65, 123.53, 123.40, 122.98; HRMS (FAB-MS, *m/z*): calcd. for C<sub>70</sub>H<sub>46</sub>, 886.3600; found, 886.3604 [M]<sup>+</sup>. Anal. calcd for C<sub>70</sub>H<sub>46</sub>: C 94.77, H 5.23; found: C 94.48, H 5.39%.

**Compound[TPB-AA-TPB] 10,10'-bis(5'-phenyl-[1,1':3',1''-terphenyl]-4-yl)-9,9'-bianthracene** compound [6] (3.0 g, 4.95 mmol), compound [3] (4.58 g, 11.88 mmol), Pd(OAc)<sub>2</sub> (0.03 g, 0.15 mmol), and tricyclohexylphosphine (0.08 g, 0.3 mmol) were added to anhydrous toluene (50 mL) and anhydrous ethanol (20 mL) solution. Then (Et)<sub>4</sub>NOH (20 wt%, 15 mL) was added to the reaction mixture at 50 °C. The mixture was refluxed for 4 h under nitrogen. After the reaction was complete, the reaction mixture was extracted with chloroform and water. The organic layer was dried with anhydrous MgSO<sub>4</sub> and filtered. The solution was evaporated. The product was isolated with silica gel column chromatography using chloroform: n-hexane (1:2) as the eluent to obtain a white solid (3.58 g, 75%). <sup>1</sup>H NMR (300 MHz, [D<sub>8</sub>]THF, 25 °C): δ (ppm) 8.19–8.13 (m, 8H), 7.98 (s, 2H), 7.94 (s, 2H), 7.91–7.87 (m, 10H), 7.78 (d, *J* = 8.4, 4H), 7.51 (t, *J* = 7.2, 8H), 7.42–7.34 (m, 8H), 7.24–7.15 (m, 8H); <sup>13</sup>C NMR (75 MHz, [D<sub>8</sub>]THF, 25 °C): δ (ppm) 143.00, 143.48, 141.67, 141.11, 138.90, 138.12, 133.96, 132.40, 131.97, 130.76, 129.21, 127.92, 127.69, 127.63, 127.40, 126.05, 125.79; HRMS (FAB-MS, *m/z*): calcd. for C<sub>76</sub>H<sub>50</sub>, 962.3913; found, 962.3905 [M]<sup>+</sup>. Anal. calcd for C<sub>76</sub>H<sub>50</sub>: C 94.77, H 5.23; found: C 93.44, H 5.24%.

**Compound[TP-AA-DPA] 10'-([1,1':3',1''-terphenyl]-5'-yl)-N,N-diphenyl-[9,9'-bianthracen]-10-amine** compound [10] (0.87 g, 1.32 mmol), diphenylamine (0.27 g, 1.58 mmol), Pd(OAc)<sub>2</sub> (0.009 g, 0.04 mmol), sodium tert-butoxide (0.38 g, 3.95 mmol), and 1.0 M tri-*tert*-butylphosphine in toluene (0.08 mL) were added to anhydrous toluene (180 mL) solution under nitrogen. After the reaction was complete, the reaction mixture was extracted with EA and water. The organic layer was dried with anhydrous MgSO<sub>4</sub> and filtered. The solution was evaporated. The product was isolated

with silica gel column chromatography using toluene: n-hexane (1:3) as the eluent to obtain a white solid (0.26 g, 26%) <sup>1</sup>H NMR (300 MHz, [D<sub>6</sub>]DMSO, 25 °C): δ (ppm) 8.25–8.22 (m, 3H), 7.98–7.90 (m, 8H), 7.55–7.41 (m, 10H), 7.33–7.24 (m, 8H), 7.19–7.11 (m, 8H), 6.97 (t, *J* = 7.2, 2H); HRMS (FAB-MS, *m/z*): calcd. for C<sub>58</sub>H<sub>39</sub>N, 749.3083; found, 749.3082 [M]<sup>+</sup>. Anal. calcd for C<sub>58</sub>H<sub>39</sub>N: C 92.89, H 5.24, N 1.87; found: C 92.50, H 5.48, N 1.83%.

**Compound[TP-AA-TPA] 4-(10'-([1,1':3',1''-terphenyl]-5'-yl)-[9,9'-bianthracen]-10-yl)-N,N-diphenylaniline** compound [10] (1.57 g, 2.39 mmol), compound [13] (0.85 g, 2.86 mmol), Pd(OAc)<sub>2</sub> (0.032 g, 0.14 mmol), and tricyclohexylphosphine (0.04 g, 0.14 mmol) were added to anhydrous THF (110 mL) solution. Then, (Et)<sub>4</sub>NOH (20 wt%, 11 mL) was added to the reaction mixture at 50 °C. The mixture was refluxed for 1 h under nitrogen. After the reaction was finished, the reaction mixture was extracted with chloroform and water. The organic layer was dried with anhydrous MgSO<sub>4</sub> and filtered. The solution was evaporated. The product was isolated with silica gel column chromatography using chloroform: n-hexane (1:6) as the eluent to obtain a white solid (0.59 g, 30%). <sup>1</sup>H NMR (300 MHz, [D<sub>8</sub>]THF, 25 °C): δ (ppm) 8.21 (s, 1H), 7.99 (d, *J* = 9.0, 4H), 7.94 (s, 2H), 7.90 (d, *J* = 7.2, 4H), 7.51–7.46 (m, 6H), 7.40–7.27 (m, 16H), 7.21–7.06 (m, 10H); HRMS (FAB-MS, *m/z*): calcd. for C<sub>64</sub>H<sub>43</sub>N, 825.3396; found, 825.3394 [M]<sup>+</sup>. Anal. calcd for C<sub>64</sub>H<sub>43</sub>N: C 93.06, H 5.25, N 1.70; found: C 92.66, H 5.24, N 1.69%.

**Compound[TPB-AA-TPA] N,N-diphenyl-4-(10'-(5'-phenyl-[1,1':3',1''-terphenyl]-4-yl)-[9,9'-bianthracen]-10-yl)aniline** compound [12] (0.5 g, 0.68 mmol), compound [13] (0.26 g, 0.82 mmol), Pd(OAc)<sub>2</sub> (0.012 g, 0.054 mmol), and tricyclohexylphosphine (0.015 g, 0.054 mmol) were added to anhydrous THF (130 mL) solution. Then, (Et)<sub>4</sub>NOH (20 wt%, 14 mL) was added to the reaction mixture at 50 °C. The mixture was refluxed for 3 h under nitrogen. After the reaction was complete, the reaction mixture was extracted with chloroform and water. The organic layer was dried with anhydrous MgSO<sub>4</sub> and filtered. The solution was evaporated. The product was isolated with silica gel column chromatography using toluene: n-hexane (1:2) as the eluent to obtain a beige solid (0.50 g, 81%). <sup>1</sup>H NMR (300 MHz, [D<sub>6</sub>]DMSO, 25 °C): δ (ppm) 8.27 (d, *J* = 8.4, 2H), 8.16 (s, 2H), 7.99 (d, *J* = 8.1, 5H), 7.90 (t, *J* = 8.7, 4H), 7.80 (d, *J* = 8.4, 2H), 7.58–7.41 (m, 16H), 7.31–7.25 (m, 10H), 7.18 (t, *J* = 2.1, 2H), 7.13 (d, *J* = 9.0, 4H); HRMS (FAB-MS, *m/z*): calcd. for C<sub>70</sub>H<sub>47</sub>N, 901.3709; found, 901.3712 [M]<sup>+</sup>. Anal. calcd for C<sub>70</sub>H<sub>47</sub>N: C 93.20, H 5.25, N 1.55; found: C 92.97, H 5.28, N 1.62%.

## 2.2. Measurements and OLED fabrication

Reagents and solvents were purchased as reagent grade and used without further purification. Analytical TLC was carried out on Merck 60 F254 silica gel plate, and column chromatography was performed on Merck 60 silica gel (230–400 mesh). The <sup>1</sup>H NMR and <sup>13</sup>C NMR spectra were recorded on Bruker Avance 300 spectrometers. The FAB+–mass and EI+–spectra were recorded on a JMS-600W, JMS-700, 6890 Series and Flash1112, Flash2000. The optical UV-Vis absorption spectra were obtained using a Lambda 1050 UV/Vis/NIR spectrometer (Perkin Elmer). A Perkin-Elmer luminescence spectrometer LS55 (Xenon flash tube) was used to perform PL spectroscopy. The glass transition temperatures (*T*<sub>g</sub>) of the compounds were DSC under a nitrogen atmosphere using a DSC 4000 (Perkin Elmer). Samples were heated to 360 °C or 400 °C at a rate of 10 °C/min, cooled at 10 °C/min, and then heated again under the same heating condition used in the initial heating process. *T*<sub>d</sub> of the compounds were measured with TGA using a TGA4000 (Perkin Elmer). Samples were heated to 800 °C at a rate of 10 °C/min. The HOMO energy levels were determined with ultraviolet photoelectron yield spectroscopy (Riken Keiki AC-2). The LUMO energy levels were derived from the HOMO energy levels and the band gaps. For

the EL devices, all organic layers were deposited under  $10^{-6}$  torr, with a rate of deposition of  $1 \text{ \AA/s}$  to give an emitting area of  $4 \text{ mm}^2$ . The LiF and aluminum layers were continuously deposited under the same vacuum conditions. The current-voltage-luminance (I-V-L) characteristics of the fabricated EL devices were obtained with a Keithley 2400 electrometer. Light intensities were obtained with a Minolta CS-1000A. To calibrate the EQE values considering the angular dependence, emission angular distributions were also measured. The operational stabilities of the devices were measured under encapsulation in a glovebox. Delayed fluorescence under electrical pulse excitations was measured using a function generator (Agilent 33220A) and an amplified Si photodetector (Thorlabs PDA8A).

### 3. Results and discussion

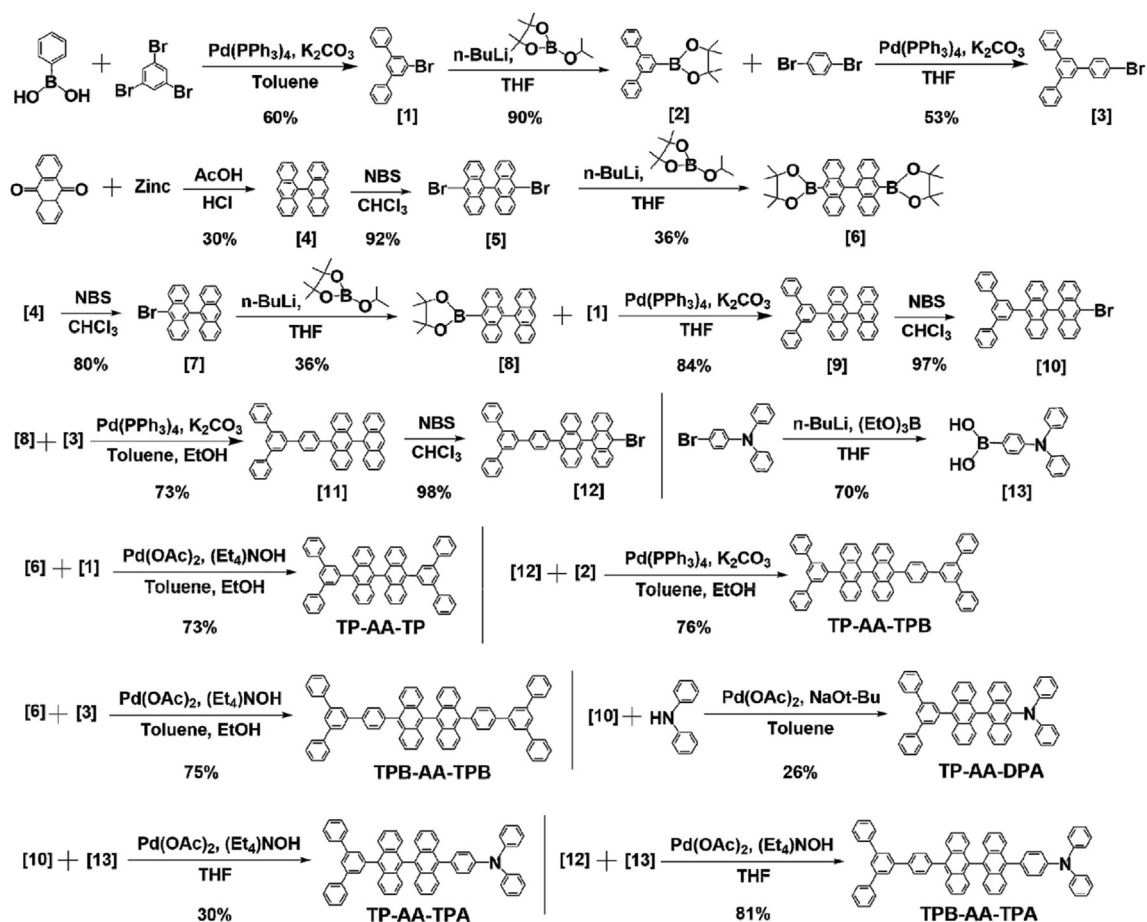
#### 3.1. Synthesis and optical properties

AA dual core was prepared by reduction coupling of 9-anthraquinone using zinc, and other reactions used boronylation, bromination, and Suzuki aryl-aryl coupling reactions. The synthesis methods are described in more detail in Scheme 2 and the experimental section. All synthesized materials were purified with reprecipitation and the column chromatography method. The synthesized compounds were characterized using nuclear magnetic resonance (NMR) spectroscopy, elemental analysis, and FAB mass analysis.

The optical and thermal properties of the synthesized materials

are summarized in Fig. 1 and Table 1. In the solution and film states, the ultraviolet-visible (UV-Vis) absorption shapes of the six synthesized materials, which have the intrinsic pattern of anthracene, mainly presented in the range of  $360 \text{ nm}$ – $410 \text{ nm}$  (Fig. 1). The highly twisted structure prevents increase in the conjugation length of AA itself so that the UV-Vis absorption spectrum and the PL spectrum of AA derivative are similar to those of a single anthracene core derivative [9,10,22]. Unlike the other five materials, TP-AA-DPA(4) had a different UV-Vis absorption peak at approximately  $450 \text{ nm}$  in the solution and film states. This is thought to be the UV-Vis absorption peak due to the intramolecular charge transfer, which occurs only when the aromatic amine group is directly substituted in anthracene [26–30].

In solution state, TP-AA-TP(1), TP-AA-TPB(2), and TPB-AA-TPB(3) (Type (A)), the PL maximum values were similar, with the values of  $434$ ,  $433$ , and  $433 \text{ nm}$ , respectively. In the cases of TP-AA-DPA(4), TP-AA-TPA(5), and TPB-AA-TPA(6) (Type (B)), the PL maximum values of  $494$ ,  $458$ , and  $458 \text{ nm}$ , respectively, were red-shifted compared to those of Type (A). We can compare the PL maximum values of Type (A) with an aromatic ring composed of only carbon and hydrogen as a side group and those of Type (B) in which an amine group is substituted for the phenyl ring of Type (A). In solution state, TP-AA-DPA(4) was red-shifted approximately  $60 \text{ nm}$  compared to TP-AA-TP(1), and TP-AA-TPA(5) and TPB-AA-TPA(6) were red-shifted approximately  $25 \text{ nm}$  compared to TP-AA-TPB(2) and TPB-AA-TPB(3). This is interpreted to be a result of the electron donating effect of the substituted aromatic amine side groups. In the case of TP-AA-DPA(4), in which DPA was substituted



Scheme 2. Synthetic routes of synthesized compounds.

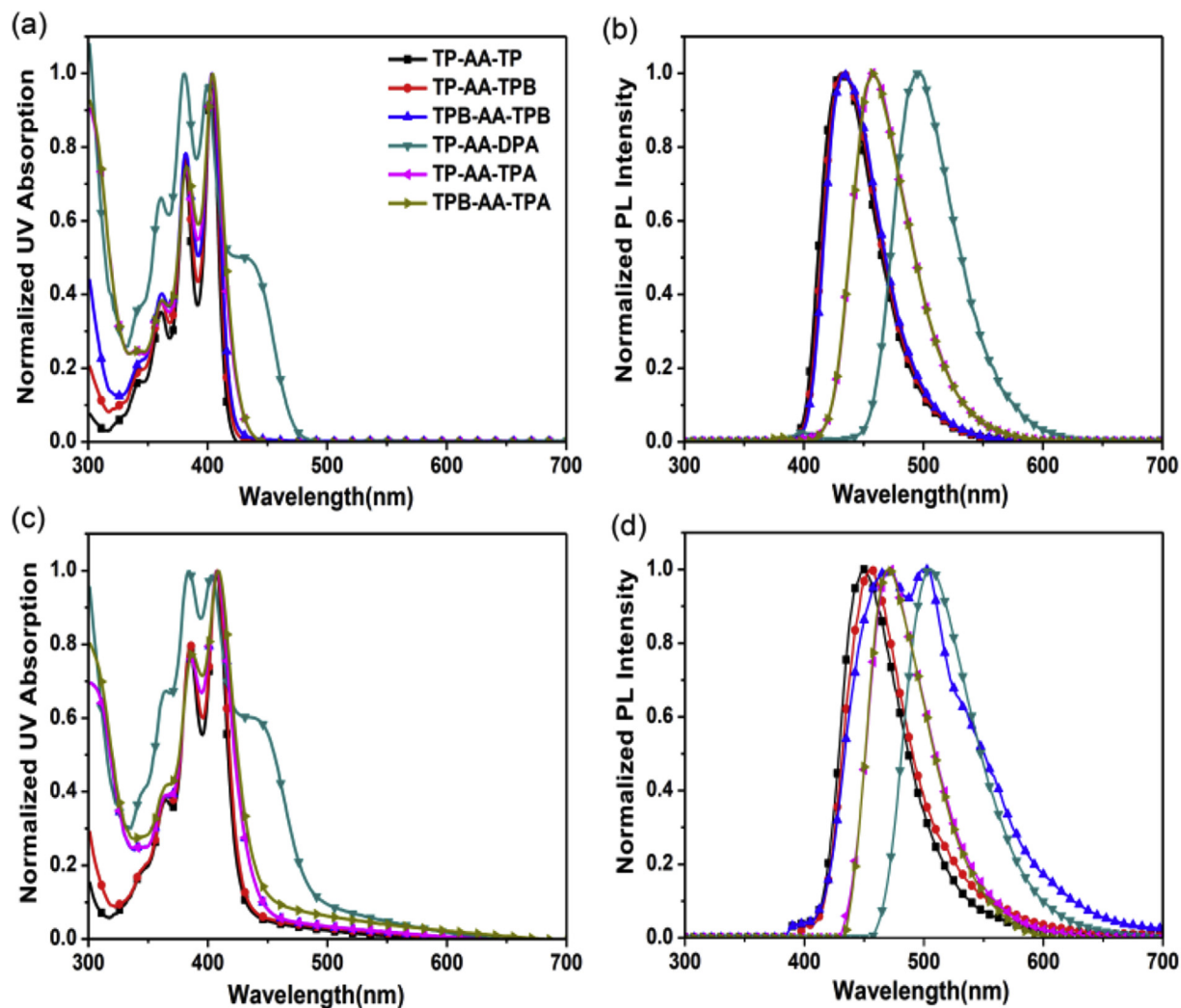


Fig. 1. UV-Vis absorption spectra and PL spectra of synthesized materials: (a) and (b)  $1.0 \times 10^{-5}$  M toluene solution; (c) and (d) vacuum-deposited film state.

Table 1

Optical and thermal properties of the synthesized materials.

Compounds	Solution <sup>a</sup>		Film on glass <sup>b</sup>		HO MO <sup>c</sup> (eV)	LU MO (eV)	Band gap (eV)	T <sub>g</sub> (°C)	T <sub>m</sub> (°C)	T <sub>d</sub> (°C)
	UV (nm)	PL (nm)	UV (nm)	PL (nm)						
TP-AA-TP	361,381,403	434	365,385,407	449	-5.78	-2.88	2.90	176	427	465
TP-AA-TPB	361,381,403	433	366,386,408	453	-5.68	-2.78	2.90	203	418	516
TPB-AA-TPB	361,382,404	433	366,386,408	464,499	-5.68	-2.79	2.89	206	425	525
TP-AA-DPA	361,380,400,444	494	365,384,403,450	503	-5.61	-3.05	2.56	192	424	425
TP-AA-TPA	361,382,404	458	366,386,408	469	-5.59	-2.86	2.73	—	335	470
TPB-AA-TPA	362,382,404	458	367,387,409	469	-5.60	-2.85	2.75	—	371	520

<sup>a</sup>  $1.00 \times 10^{-5}$  M toluene solution.

<sup>b</sup> Film thickness is 50 nm on the glass.

<sup>c</sup> Ultraviolet photoelectron spectroscopy.

to maximize the electron donating effect in the AA core, the PL maximum value was the most highly red-shifted. However, when TPA was substituted, one phenyl ring was positioned between the core and the DPA side group, resulting in a reduction of the electron donating effect of DPA and a smaller red-shift of substituted DPA.

Generally, the PL maximum value in the film state is red-shifted as the distance between the molecules becomes closer than in the solution state. The film PL maximum values of TP-AA-TP(1), TP-AA-

TPB(2), and TPB-AA-TPB(3) were 449, 453, and 464 nm, respectively. The PL maximum values for the film state of TP-AA-TP(1), TP-AA-TPB(2), and TPB-AA-TPB(3) were red-shifted by 15, 20, and 31 nm compared to the PL maximum values of the solution state. In addition, when the substituted side group was changed from TP to TPB, the intermolecular conjugation length was increased by the added phenyl ring in the side group, and the PL maximum value shifted from 449 nm to 453 nm and 464 nm. TPB-AA-TPB(3)

showed the emission of the excimer peak at 499 nm in addition to 464 nm. When the size of the side group is properly matched with the size of the whole molecule, the excimer may be generated in the film state, inducing the orientation of the molecule, which was shown previously [20]. PL spectra change with increasing concentration, excitation spectra, and time-resolved PL measurement experiments were analyzed to confirm that 499 nm of TPB-AA-TPB(3) was excimer emission peak.

Firstly, using toluene, PL spectra change at concentrations from  $1.0 \times 10^{-5}$  M to  $1.0 \times 10^{-2}$  M was measured (Fig. S1, ESI). The excimer peak is not seen at the diluted concentration (ex:  $1.0 \times 10^{-5}$  M); however, as the concentration increases, intermolecular aggregation,  $\pi$ - $\pi$  electron stacking, and the excimer peak would occur [31,32]. PL maximum value of TPB-AA-TPB(3) was red-shifted from 433 nm to 462 nm as the concentration increases, and the excimer peak at 490 nm can be simultaneously observed from  $2.5 \times 10^{-3}$  M. Secondly, the excitation spectra of TPB-AA-TPB(3) in the film state were measured. Excitation spectra were measured along with the UV-Vis absorption spectrum (Fig. S2, ESI). The UV-Vis absorption spectrum matched well with the excitation spectra. The excitation spectra monitored at 464 nm and 499 nm are very similar, indicating that they arise from the same excitation pathway. Thirdly, time-resolved PL was measured when TPB-AA-TPB(3) was in the film state. The excimer generally has a longer decay lifetime than the original peak material [33]. The average decay rate of TPB-AA-TPB(3) was 0.93 ns at 464 nm and 2.03 ns at 499 nm, and the decay lifetime at 499 nm was relatively longer (Fig. S3, ESI) [19–21]. From these three experimental results, PL emission at 499 nm for TPB-AA-TPB(3) was determined to be the excimer peak.

In the film states of TP-AA-DPA(4), TP-AA-TPA(5), and TPB-AA-TPA(6), which are Type (B), the PL maximum value was red shifted from that of Type (A) and showed PL maximum values at 503 nm, 469 nm, and 469 nm, respectively. This trend was similar to that seen in the solution state. When the film PL maximum values were compared with the solution PL maximum values of Type (B), they were red-shifted 9 nm–11 nm. It was relatively red-shifted less than Type (A) which was approximately red-shifted 15 nm–31 nm. Since Type (B) with a polar aromatic amine side group has different interactions depending on the polarity of solvent compared to Type (A), a change in the PL maximum value mainly occurs in the solution state [10].

When the film PL maximum values of Type(A) and Type (B) were compared, TP-AA-DPA(4) was red-shifted approximately 54 nm compared to TP-AA-TP(1). TP-AA-TPA(5) and TPB-AA-TPA(6) were red-shifted approximately 16 nm and 5 nm compared to TP-AA-TPB(2) and TPB-AA-TPB(3), respectively. This is due to the electron donating effect of the substituted aromatic amine side group. When DPA is substituted, it is the most red-shifted, and TP-AA-DPA(4) emitted in the green region. When replacing TPA, the donating effect of electrons is slightly reduced compared to DPA due to the phenyl ring substituting directly to the core, and it is not significantly red-shifted. Therefore, TP-AA-TPA(5) and TPB-AA-TPA(6) were able to maintain emission in the blue region, similar to Type (A).

### 3.2. Electrical and thermal properties

The HOMO levels were determined by photoelectron spectroscopy using an ultraviolet light energy source. The LUMO energy levels were obtained from the HOMO levels and the optical band gaps (Table 1). The optical band gaps were derived by determining the absorption edges from plots of  $(\alpha h\nu)$  vs.  $(\alpha h\nu)^2$ , where  $\alpha$ ,  $h$ , and  $\nu$  are the absorbance, Planck's constant, and the frequency of light, respectively. The glass transition temperatures ( $T_g$ ), the melting

temperatures ( $T_m$ ) and the decomposition temperatures ( $T_d$ ) of the synthesized materials were determined with differential scanning calorimetry (DSC) and thermogravimetric analysis (TGA) as shown in Table 1.

In the case of Type (A), HOMO level was  $-5.68$  eV to  $-5.78$  eV, while that of Type (B) was  $-5.59$  eV to  $-5.61$  eV. When Type (A) and Type (B) were compared, Type (B) had a  $0.09$  eV– $0.17$  eV higher HOMO level than that of Type (A). This is the result of the increased electron donating effect of the aromatic amine group acting on Type (B).

The  $T_d$  values of the six synthesized material showed that the higher was the molecular weight, the higher was the  $T_d$  value. The order of molecular weight for Type (A) is TPB-AA-TPB(3) > (2)TP-AA-TPB > TP-AA-TP(1), and that of  $T_d$  values is  $525$  °C >  $516$  °C >  $465$  °C. In the case of Type (B), the molecular weights were determined to be in the order of TPB-AA-TPA(6) > TP-AA-TPA(5) > TP-AA-DPA(4), and  $T_d$  values were in the order of  $520$  °C >  $470$  °C >  $425$  °C. All  $T_d$  values of the synthesized materials showed high thermal stability with a minimum value of  $425$  °C. The  $T_d$  values of these materials showed an increase of  $28$  °C– $128$  °C above the  $T_d$  value of  $397$  °C for MADN, which is one of the commercially used blue emitting materials.

$T_m$  values of the six synthesized materials had a minimum of  $335$  °C, and  $T_g$  values were high at a minimum of  $176$  °C. It was confirmed that the six materials had higher  $T_m$  values by a minimum of  $80$  °C and  $T_g$  values by a minimum of  $56$  °C than those of MADN, which has a  $T_m$  of  $255$  °C and  $T_g$  of  $120$  °C. In Type (A),  $T_m$  values of TP-AA-TP(1) and TPB-AA-TPB(3), which has symmetric side groups, were  $427$  °C and  $425$  °C, respectively. These are higher than the  $T_m$  of  $418$  °C for TP-AA-TPB(2), which has an asymmetric side group. This difference comes from the symmetry of the molecules.

The  $T_g$  value increased to  $176$  °C,  $203$  °C, and  $206$  °C for TP-AA-TP(1), TP-AA-TPB(2), and TPB-AA-TPB(3), respectively, as the molecular weight increased. When the  $T_g$  values of TP-AA-TP(1) and TP-AA-DPA(4) were compared, TP-AA-DPA(4) was approximately  $191$  °C, which was higher by approximately  $15$  °C than the  $T_g$  value of TP-AA-TP(1). This is presumably due to the generated dipole in the TP-AA-DPA(4) molecule. It is thought that these highly thermal characteristics can implement a stable device whose morphology does not easily change due to the heat generated from the operation of OLED device [34].

### 3.3. Electroluminescence properties

Using the six synthesized materials as an emitting layer (EML), a non-doped device was fabricated with the following structure: ITO/tris(N-(naphthalen-2-yl)-N-phenyl-amino)triphenylamine (2-TNATA) (60 nm)/N,N'-bis(naphthalen-1-yl)-N,N'-bis(phenyl)benzidine (NPB) (15 nm)/EML (synthesized compounds, 30 nm)/8-hydroxyquinoline aluminum (Alq<sub>3</sub>) (15 nm)/LiF (1 nm)/Al (200 nm). Here, 2-TNATA was used as the hole injection layer (HIL), and NPB was used as the hole transporting layer (HTL). Alq<sub>3</sub> was used as the electron transporting layer (ETL), LiF as the electron injection layer (EIL), and ITO and Al were used as the anode and cathode, respectively. The measured EL results are summarized in Table 2.

Overall, the operating voltage of Type (B) was lower than that of Type (A). This is because the difference in HOMO energy level between NPB used as the HTL and Type (B) was  $0.19$  eV– $0.21$  eV and was less than the  $0.28$  eV– $0.38$  eV difference between NPB and Type (A). It is easy to induce hole injection from NPB to Type (B). Also, the difference in LUMO energy level between Alq<sub>3</sub> used as the ETL and Type (B) was  $0.05$  eV– $0.14$  eV and was less than the  $0.12$  eV– $0.23$  eV difference between Alq<sub>3</sub> and Type (A). It is also

**Table 2**

EL performances: ITO/2-TNATA (60 nm)/NPB (15 nm)/EML (30 nm)/Alq<sub>3</sub> (15 nm)/LiF (1 nm)/Al (200 nm) at 10 mA/cm<sup>2</sup>.

EMLs	Operating voltage (V)	EL <sub>max</sub> (nm)	Current efficiency (cd/A)	Power efficiency (lm/W)	EQE (%)	CIE (x,y)
TP-AA-TP	7.33	450	4.27	2.00	4.26	(0.15,0.12)
TP-AA-TPB	7.69	455	5.10	2.33	4.02	(0.17,0.15)
TPB-AA-TPB	8.15	469,499	2.72	1.14	1.50	(0.21,0.29)
TP-AA-DPA	7.08	501	7.79	3.79	3.17	(0.19,0.52)
TP-AA-TPA	6.66	466	6.78	3.55	4.71	(0.15,0.20)
TPB-AA-TPA	7.00	466	8.97	4.43	6.37	(0.14,0.19)

easier to induce electron injection from Alq<sub>3</sub> to Type (B) than Type (A) (Fig. 2(a)).

Comparing the EL maximum value with the PL maximum value showed a similar range of 450 nm–501 nm. In the case of TPB-AA-TPB(3), the excimer band appeared at 499 nm, as in the PL spectrum, and all materials excluding TP-AA-DPA(4) showed an EL spectrum in the blue region (Fig. 2(b)).

The results of EL efficiencies and Commission Internationale de L'Eclairage coordinates (CIE) are as follows. For Type (A), TP-AA-TP(1) showed a current efficiency of 4.27 cd/A, power efficiency of 2.00 lm/W, and external quantum efficiency (EQE) of 4.26%. TP-AA-TPB(2) had a current efficiency of 5.10 cd/A, which is about 1.2 times higher than that of TP-AA-TP(1), power efficiency of 2.33 lm/W, and EQE of 4.02% (Fig. 3).

This is because TPB with a larger size than TP shows the bulky size effect of side group. Also, due to the higher relative PL quantum efficiency of TPB than that of TP, TP-AA-TPB(2) has a higher current efficiency than TP-AA-TP(1) [9,19,35,36]. As a result, the power efficiency of TP-AA-TPB(2) was also increased compared to TP-AA-TP(1).

TPB-AA-TPB(3) had a current efficiency of 2.72 cd/A, power efficiency of 1.14 lm/W, and EQE of 1.50%. This material showed an excimer peak in both the EL spectrum and the PL spectrum. In general, the material that shows an excimer has low EL efficiency, and it can be interpreted as indicating many non-radiative decay pathways [37–39]. Therefore, in the case of TPB-AA-TPB(3), the three kinds of device EL efficiencies are low.

For Type (B), TP-AA-DPA(4) showed a high current efficiency of 7.79 cd/A, power efficiency of 3.79 lm/W, and EQE of 3.17% due to the electron donating effect of the aromatic amine side group. However, with the strong donating effect of the side group, the EL maximum and CIE values were 501 nm and (0.19, 0.52) indicating

green color as the film PL.

TP-AA-TPA(5) showed relatively lower efficiency than TP-AA-DPA(4), with a current efficiency of 6.78 cd/A, power efficiency of 3.55 lm/W, and EQE of 4.72%. However, the weak donating effect of the side group made it possible to maintain the emission of the blue region with an EL maximum value of 466 nm and CIE of (0.15, 0.20). TPB-AA-TPA(6) showed the highest efficiency among the six synthesized materials, with a current efficiency of 8.97 cd/A, power efficiency of 4.43 lm/W, and EQE of 6.37%. And the EL maximum and CIE values of TPB-AA-TPA(6) was 466 nm and (0.14, 0.19), which is blue emission. This result came from that the electron donating effect and the size effect of the side group were optimized.

These EL results of synthesized materials overall showed high performance. Especially, TPB-AA-TPA(6) has higher EL efficiency compared to previous studies using AA core. Z. Li et al. and Y. Yu et al. reported blue emitting materials with a current efficiency of 3.05 cd/A and EQE of 5.02% by introducing fluoro and trifluoromethyl electron withdrawing side groups in AA derivatives [40–42]. P. Zhang et al. introduced the chromophore, carbazole, as a side group on the AA to obtain a current efficiency of 3.2 cd/A and EQE of 3.4% and J.Y. Song et al. developed AA derivatives substituted with triphenylsilane with a current efficiency of 2.76 cd/A and EQE of 1.82% [43,44].

Comparing TP-AA-TP(1) with TP-AA-DPA(4), the EL efficiency of TP-AA-DPA(4) is 1.8 times higher than that of TP-AA-TP(1) because it increased due to the electron donating effect of the aromatic amine side group. However, the EL maximum value of TP-AA-DPA(4) is red-shifted 51 nm, and using DPA as a side group in the AA core can increase the EL efficiency but presents difficulties with blue emission [10,19]. Thus, it is necessary to add one or more phenyl rings between the core and the side group in order to optimize the electron donating effect and maintain the blue emission. As a result, when TP-AA-TPA(5) is compared with TP-AA-DPA(4), TP-AA-TPA(5) is blue-shifted 35 nm and has an EL maximum value at 466 nm.

Also, comparing TP-AA-TPB(2) with TPB-AA-TPA(5), the EL maximum value of TP-AA-TPA(5) was red-shifted 11 nm, but blue emission could still be maintained, and the EL efficiency of TP-AA-TPA(5) increased 1.3 times compared to the value of TP-AA-TPB(2). Comparison of TPB-AA-TPB(3) and TPB-AA-TPA(6) showed that TPB-AA-TPA(6) was increased the current efficiency by 3.2 times compared to that of TPB-AA-TPB(3). The efficiency of TPB-AA-TPA(6) was increased by preventing the excimer from asymmetrically replacing side groups and optimizing the electron donating effect of the side group. When TPB-AA-TPA(6) was compared with

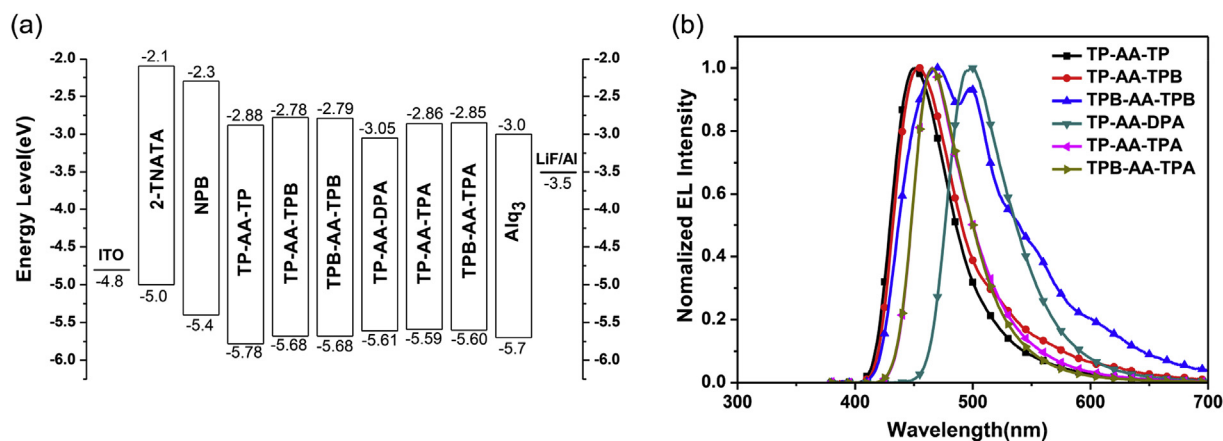
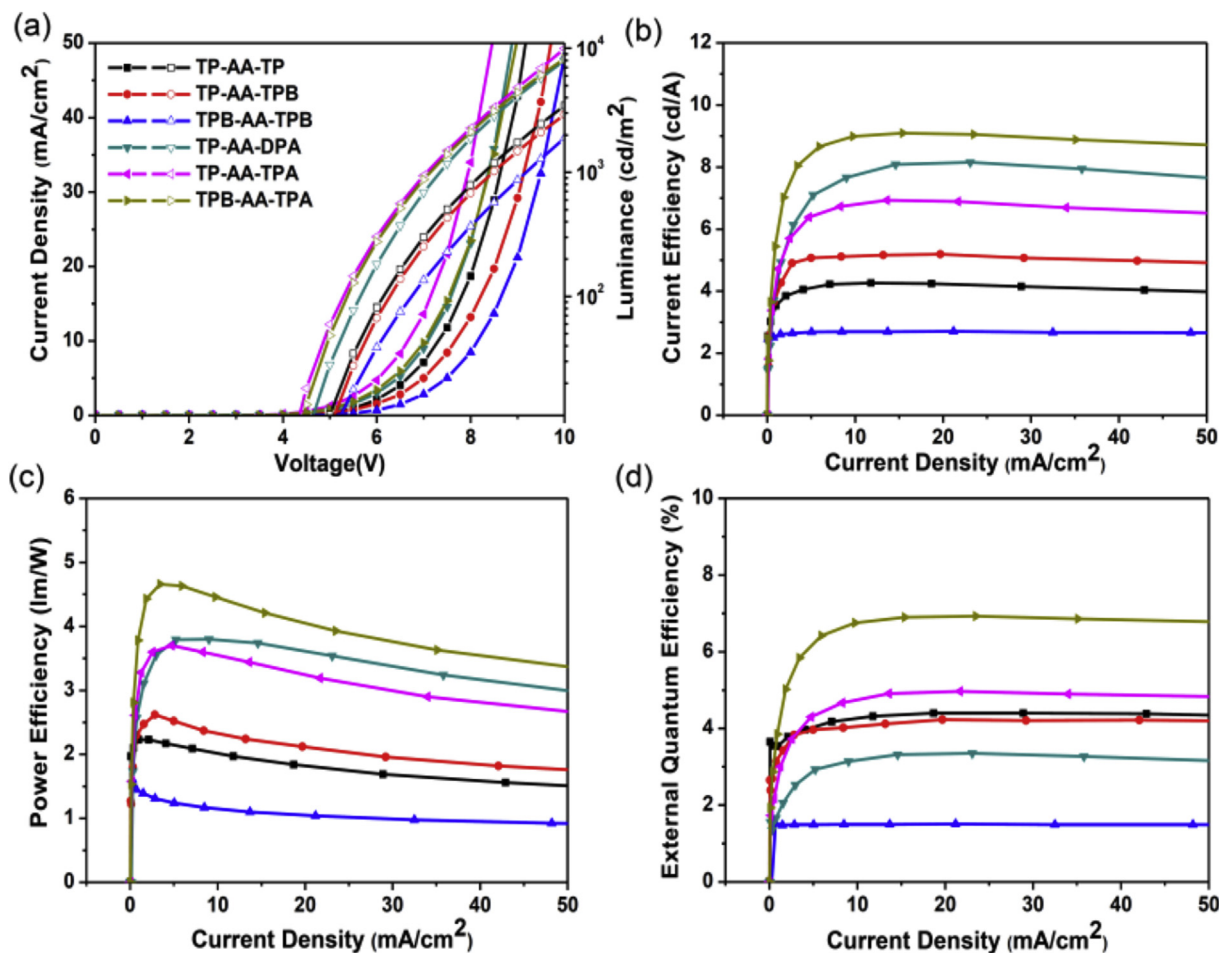


Fig. 2. EL characteristics of devices using the synthetic materials as EML: (a) energy diagram and (b) EL spectra.



**Fig. 3.** EL characteristics of devices using the synthetic materials as EML: (a) I–V–L character, (b) current efficiency against current density, (c) power efficiency against current density, and (d) external quantum efficiency against current density.

TP-AA-TPA(5), TPB-AA-TPA(6) was increased the efficiency approximately 1.2 times higher than TP-AA-TPA(5). This is because TPB has not only a larger side group size than TP, more efficiently prevents intermolecular packing, but also the higher relative PL quantum efficiency of TPB than that of TP [9,19,35,36].

Materials substituted with TPA in this series as a whole showed high EL efficiency, especially for maintaining blue emission. That is, when TPA, which is an aromatic amine side group, is substituted on the AA core, the EL efficiency can be increased, and blue emission can be maintained. Further, by replacing the bulky aromatic side group of TPB with relatively high PL quantum efficiency, the EL efficiency of the final molecule can be increased. Therefore, TPB-AA-TPA(6) was maximized the EL efficiency using the AA core by optimizing side groups for blue emitting materials.

#### 4. Conclusions

In this study, we synthesized six materials by systematically changing the side groups on the AA core and optimized EL emission wavelength and EL efficiency. TP-AA-TP(1), TP-AA-TPB(2), and TPB-AA-TPB(3) of Type (A), which are composed of only carbon and hydrogen, and TP-AA-DPA(4), TP-AA-TPA(5), and TPB-AA-TPA(6) of Type (B), which have substituted aromatic amine groups as side groups. Type (B) showed higher overall EL efficiency than Type (A) due to the electron donating effect of the substituted aromatic amine side group. Particularly, TPB-AA-TPA(6) with a bulky size

group and aromatic amine side group, showed not only blue emission but also the highest EL efficiency among the six synthesized materials with a current efficiency of 8.97 cd/A, power efficiency of 4.43 lm/W, and EQE of 6.37%. The results show that the size and electron donating effect of the side group were optimized. Studies of such systematic changes between the core and side groups of molecular structures will help to increase EL efficiency and obtain optimized OLED data.

#### Acknowledgements

This research was supported by a grant from the Technology Development Program for Strategic Core Materials funded by the Ministry of Trade, Industry & Energy, Republic of Korea (Project No. 10047758). This research was supported by Basic Science Research Program through the National Research Foundation of Korea funded by the Ministry of Education (No. 2016R1D1A1B03931477).

#### Appendix A. Supplementary data

Supplementary data related to this article can be found at <http://dx.doi.org/10.1016/j.dyepig.2017.06.053>.

#### References

- [1] Tang CW, Vanslyke SA. Organic electroluminescent diodes. *Appl Phys Lett* 1987;51:913.

- [2] Lee S, Kim KH, Limbach D, Park YS, Kim JJ. Low roll-off and high efficiency orange organic light emitting diodes with controlled co-doping of green and red phosphorescent dopants in an exciplex forming co-host. *Adv Funct Mater* 2013;23:4105–10.
- [3] Kuei CY, Tsai WL, Tong B, Jiao M, Lee WK, Chi Y, et al. Bis-tridentate Ir(III) complexes with nearly unitary RGB phosphorescence and organic light-emitting diodes with external quantum efficiency exceeding 31 %. *Adv Mater* 2016;28:2795–800.
- [4] Giridhar T, Han TH, Cho W, Saravanan C, Lee TW, Jin SH. An easy route to red emitting homoleptic Ir<sup>III</sup> complex for highly efficient solution-processed phosphorescent organic light-emitting diodes. *Chem Eur J* 2014;20:8260–4.
- [5] Uoyama H, Goushi K, Shizu K, Nomura H, Adachi C. Highly efficient organic light-emitting diodes from delayed fluorescence. *Nature* 2012;492:234–8.
- [6] Fleetham T, Ecton J, Li G, Li J. Improved out-coupling efficiency from a green microcavity OLED with a narrow band emission source. *Org Electron* 2016;37:141–7.
- [7] Komatsu R, Sasabe H, Seino Y, Nakao K, Kido J. Light-blue thermally activated delayed fluorescent emitters realizing a high external quantum efficiency of 25% and unprecedented low drive voltages in OLEDs. *J Mater Chem C* 2016;4:2274–8.
- [8] Zhang D, Cai M, Bin Z, Zhang Y, Zhang D, Duan L. Highly efficient blue thermally activated delayed fluorescent OLEDs with record-low driving voltages utilizing high triplet energy hosts with small singlet–triplet splittings. *Chem Sci* 2016;7:3355–63.
- [9] Kim SK, Yang B, Ma Y, Lee JH, Park J. Exceedingly efficient deep-blue electroluminescence from new anthracenes obtained using rational molecular design. *J Mater Chem* 2008;18:3376–84.
- [10] Kim SK, Yang B, Park YI, Ma Y, Lee JY, Kim HJ, et al. Synthesis and electroluminescent properties of highly efficient anthracene derivatives with bulky side groups. *Org Electron* 2009;10:822–33.
- [11] Kim B, Park Y, Lee J, Yokoyama D, Lee JH, Kido J, et al. Synthesis and electroluminescence properties of highly efficient blue fluorescence emitters using dual core chromophores. *J Mater Chem C* 2013;1:432–40.
- [12] Lee H, Kim B, Kim S, Kim J, Lee J, Shin H, et al. Synthesis and electroluminescence properties of highly efficient dual core chromophores with side groups for blue emission. *J Mater Chem C* 2014;2:4737–47.
- [13] Reddy SS, Cho W, Sree VG, Jin SH. Multi-functional highly efficient bipolar 9,9-dimethyl-9,10-dihydroacridine/imidazole-based materials for solution-processed organic light-emitting diode applications. *Dyes Pigm* 2016;134:315–24.
- [14] Reddy SS, Sree VG, Gunasekar K, Cho W, Gal YS, Song M, et al. Highly efficient bipolar deep-blue fluorescent emitters for solution-processed non-doped organic light-emitting diodes based on 9,9-Dimethyl-9,10-dihydroacridine/Phenanthroimidazole derivatives. *Adv Opt Mater* 2016;4:1236–46.
- [15] Reddy SS, Sree VG, Cho W, Jin SH. Achieving pure deep-blue electroluminescence with CIE  $y < 0.06$  via a rational design approach for highly efficient non-doped solution-processed organic light-emitting diodes. *Chem Asian J* 2016;11:3275–82.
- [16] Kuma H, Hosokawa C. Blue fluorescent OLED materials and their application for high-performance devices. *Sci Technol Adv Mater* 2014;15:034201.
- [17] Goushi K, Kwong R, Brown JJ, Sasabe H, Adachi C. Triplet exciton confinement and unconfinement by adjacent hole-transport layers. *J Appl Phys* 2004;95:7798–802.
- [18] Holmes RJ, D'Andrade BW, Forrest SR, Ren X, Li J, Thompson ME. Efficient, deep-blue organic electrophosphorescence by guest charge trapping. *Appl Phys Lett* 2003;83:3818–20.
- [19] Shin H, Jung H, Kim B, Lee J, Moon J, Kim J, et al. Highly efficient emitters of ultra-deep-blue light made from chrysene chromophores. *J Mater Chem C* 2016;4:3833–42.
- [20] Lee J, Kim B, Kwon JE, Kim J, Yokoyama D, Suzuki K, et al. Excimer formation in organic emitter films associated with a molecular orientation promoted by steric hindrance. *Chem Commun* 2014;50:14145–8.
- [21] Lee J, Jung H, Shin H, Kim J, Yokoyama D, Nishimura H, et al. Excimer emission based on the control of molecular structure and intermolecular interactions. *J Mater Chem C* 2016;4:2784–92.
- [22] Sarkar M, Saman A. 10,10'-Di-bromo-9,9'-bianthryl. *Acta Crystallogr Sect E Struct Rep Online* 2003;59:o1764.
- [23] Wortmann R, Elich K, Lebus S, Liptay W. Experimental determination of the  $S_1$  torsional potential of 9,9'-bianthryl in 2-methyl-butane by simultaneous Franck–Condon and band shape analysis of temperature dependent optical fluorescence spectra. *J Chem Phys* 1991;95:6371–81.
- [24] Subaric-leitis A, Monte C, Roggan A, Rettig W, Zimmermann P, Heinze J. Torsional band assignment and intramolecular twist potential of 9,9'-bianthryl and its 10-cyano derivative in a free jet. *J Chem Phys* 1990;93:4543–55.
- [25] Grozema FC, Swart M, Zijlstra RWJ, Piet JJ, Siebbeles LDA, Van Duijnen PTH. QM/MM study of the role of the solvent in the formation of the charge separated excited state in 9,9'-bianthryl. *J Am Chem Soc* 2005;127:11019–28.
- [26] Yu MX, Duan JP, Lin CH, Cheng CH, Tao YT. Diaminoanthracene derivatives as high-performance green host electroluminescent materials. *Chem Mater* 2002;14:3958–63.
- [27] Sasaki S, Hattori K, Igawa K, Konishi GI. Directional control of  $\pi$ -conjugation enabled by distortion of the donor plane in diarylaminoanthracenes: a Photophysical Study. *J Phys Chem A* 2015;119:4898–906.
- [28] Wei X, Bu L, Li X, Ågren H, Xie Y. Full color emissions based on intramolecular charge transfer effect modulated by formyl and boron-dipyrromethene moieties. *Dyes Pigm* 2017;136:480–7.
- [29] Chen B, Yu G, Li X, Ding Y, Wang C, Liu Z, et al. Full-colour luminescent compounds based on anthracene and 2,2'-dipyridylamine. *J Mater Chem C* 2013;1:7409–17.
- [30] Rajamalli P, Gandeepan P, Huang MJ, Cheng CH. Bromo induced reversible distinct color switching of a structurally simple donor–acceptor molecule by vapo, piezo and thermal stimuli. *J Mater Chem C* 2015;3:3329–35.
- [31] Crenshaw BR, Weder C. Deformation-induced color changes in melt-processed photoluminescent polymer blends. *Chem Mater* 2003;15:4717–24.
- [32] Szadkowska-Nicze M, Wolszczak M, Kroh J, Mayer J. Concentration dependence of pyrene excimer formation in doped polyethylene. *J Photochem Photobiol A* 1993;75:125–9.
- [33] Lindquist RJ, Lefler KM, Brown KE, Dyar SM, Marglies EA, Young RM, et al. Energy flow dynamics within cofacial and slip-stacked perylene-3,4-dicarboximide dimer models of  $\pi$ -aggregates. *J Am Chem Soc* 2014;136:14912–23.
- [34] Park Y, Kim B, Lee C, Hyun A, Jang S, Lee JH, et al. Highly efficient new hole injection materials for OLEDs based on dimeric phenothiazine and phenoxazine derivatives. *J Phys Chem C* 2011;115:4843–50.
- [35] Lee H, Park YI, Kim B, Lee JH, Park J. Highly efficient blue emitting materials based on indenopyrazine derivatives for OLEDs. *Opt Mater Express* 2014;4:924–33.
- [36] Niko Y, Kawauchi S, Otsu S, Tokumaru K, Konishi GI. Fluorescence enhancement of pyrene chromophores induced by alkyl groups through  $\sigma$ - $\pi$  conjugation: systematic synthesis of primary, secondary, and tertiary alkylated pyrenes at the 1, 3, 6, and 8 positions and their photophysical properties. *J Org Chem* 2013;78:3196–207.
- [37] Brown KE, Salamant WA, Shoer LE, Young RM, Wasielewski MR. Direct observation of ultrafast excimer formation in covalent perylenedimide dimers using near-infrared transient absorption spectroscopy. *J Phys Chem Lett* 2014;5:2588–93.
- [38] Jagtap SP, Mukhopadhyay S, Coropceanu V, Brizius GL, Bredas JL, Collard DM. Closely stacked oligo(phenylene ethynylene)s: effect of  $\pi$ -stacking on the electronic properties of conjugated chromophores. *J Am Chem Soc* 2012;134:7176–85.
- [39] Luo JD, Xie ZL, Lam JWY, Cheng L, Chen HY, Qiu CF, et al. Aggregation-induced emission of 1-methyl-1,2,3,4,5-pentaphenylsilole. *Chem Commun* 2001:1740–1.
- [40] Li Z, Sun Y, Li H, Ren J, Si C, Lv X, et al. Efficient blue fluorescent electroluminescence based on a tert-butylated 9,9'-bianthracene derivative with a twisted intramolecular charge-transfer excited state. *Synth Met* 2016;217:102–8.
- [41] Li Z, Liu W, Yu Y, Lv X, Si C, Wu Z, et al. Effect of fluorocarbon (trifluoromethyl groups) substitution on blue electroluminescent properties of 9,9'-bianthracene derivatives with twisted intramolecular charge-transfer excited states. *Dyes Pigm* 2015;122:238–45.
- [42] Yu Y, Wu Z, Li Z, Jiao B, Li L, Ma L, et al. Highly efficient deep-blue organic electroluminescent devices (CIE $y \approx 0.08$ ) doped with fluorinated 9,9'-bianthracene derivatives (fluorophores). *J Mater Chem C* 2013;1:8117–27.
- [43] Zhang P, Dou W, Ju Z, Yang L, Tang X, Liu W, et al. 9,9'-bianthracene-cored molecule enjoying twisted intramolecular charge transfer to enhance radiative-excitons generation for highly efficient deep-blue OLEDs. *Org Electron* 2013;14:915–25.
- [44] Song JY, Park SN, Lee SJ, Lee YK, Yoon SS. Novel fluorescent blue-emitting materials based on anthracene-fluorene hybrids with triphenylsilane group for organic light-emitting diodes. *Dyes Pigm* 2015;114:40–6.